Population Oscillations in Excited Argon Atoms Initiated by Attosecond Pulses

Anna Olofsson

Thesis submitted for the degree of Bachelor of Science
Project duration of 2 months

Supervised by
Johan Mauritsson and Samuel Bengtsson

LUND UNIVERSITY

Department of Physics
Division of Atomic Physics
May 2016

LRAP 517

Abstract

This project aims to study the process of electron excitation by a light pulse, a process at the core of many important contemporary and possible future devices. Data from an experiment where the electron dynamics is probed with attosecond laser pulses are analyzed in order to gain insight on the rapid population oscillations within the excited atomic system and simulations are constructed with the goal of mimicking structures found in the experimental data. The results imply that the effect of a third state, which is reached by interaction with an incident pulse, on the population oscillations might explain the experimentally observed structures. Some control might be possible to exempt on the composition of the superposition state of the electron, by varying the time when the pulse is incident on the atom.

Acknowledgements

Many thanks to my supervisors and others in the research group at the attosecond physics division in Lund who let me take part in their research and found the time to provide guidance to me whenever it was needed. Also, the time spent on this project would not have been the same without the friendly atmosphere of office A209.

Contents

1 Introduction

The study and control of electrons have been part of a major field of research and have spurred many technological advances since the beginning of the nineteenth century. However, there are still plenty of things about the behavior of electrons that are yet to be discovered, for example what really happens when an atom is excited. This is partly due to the fact that electron dynamics often happens on a very short timescale, at least in room temperature, so that it has not been possible to probe the process before the state of the electron has had time to change. When technological advances enabled the creation of attosecond laser pulses, it became possible to probe the electron dynamics on a timescale where it was previously hidden.

The main discovery that enabled the production of attosecond pulses was the success in developing high harmonics generation, where a laser with a certain frequency can be manipulated so that pulses with frequencies that are the odd harmonics of the original laser frequency are obtained [1]. The scientific opportunities enabled by the existence of attosecond pulses are so many that they sparked a new field called attosecond physics.

The field of attosecond physics has recently produced insights into for example the process of tunneling; a study in 2015 used attosecond pulses to achieve the necessary temporal resolution to analyze the tunneling process by manipulating a potential barrier [2]. But attosecond pulses have also spurred interdisciplinary studies: they are a current interest of the field of biology. This is because they enable the study of molecules before the molecule is changed by rapid core ionization, which has been an obstacle for biologists when performing a microscopy of for example proteins [3].

At Lund University, the attosecond pulses have been used for a wide variety of applications. For example, they have been used together with a photoelectron emission microscope to measure nanostructures with high temporal and spatial resolution [4], [5]. They have also been used to study two-photon ionization in Helium [6] as well as interference effects between quasi-bound electron wave functions and free electron wave functions in an ionizing process [7].

A current experiment at Lund University aims at investigating the direction and spatial phase of the radiation emitted from excited Argon atoms and their dependence on a time delay between two laser pulses [8]. As found in another study of Argon ionization with attosecond pulses, internal population transfers between the eigenstates from which the coherently excited state is formed have a visible impact on the absorption spectrum [9]. These internal population transfers are what this research project aims to investigate, in collaboration with the group who performs the scattering experiment. To maintain the project at an appropriate level, it is strictly focused on this small part of the on-going experiment.

The goal of this research project is thus to study the specific aspect of an electron excitation that concerns population oscillations within a coherently excited state. This is done through connecting specific properties of the experimental data from the scattering experiment, which are believed to be caused by population transfers within the coherently excited state, to a simulation of a three-state system within an excited atom. To keep the simulation at a level appropriate for a bachelors diploma project, the simulation starts from the moment the atom becomes excited, and the timescale of the simulation is kept short enough that the states can be considered

long-lived. These two presuppositions simplify matters so that it is only the initial composition of the mixed state and the effect of a pulse that change the system.

2 Theory

To understand the interaction of light with matter, a good starting point is to this day still a concept put forward by Albert Einstein. The theory concerns the transition rates of absorption, stimulated emission and spontaneous emission, as depicted in Fig. 1; it states that the increase of electrons in the upper state with time will depend on the intensity of the field at the transition frequency, the number of electrons in the lower level, the number of available states in the upper level and certain probability constants called Einstein coefficients [10].

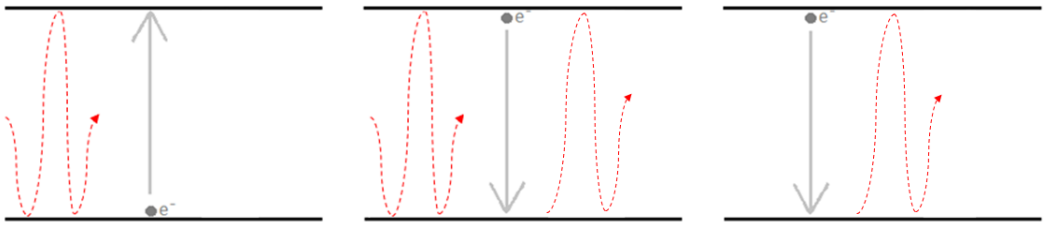

Figure 1: Schematic representation of the three basic ways a photon can affect electrons in matter according to Einstein's theory. To the left: absorption, when an electron (e^- in the figure) absorbs a photon (red broken lines in the figure) and gains an equivalent amount of energy. In the middle: stimulated emission, where an electron is stimulated by an incoming photon to de-excite and emit the energy as a photon, identical to the initial photon. Finally, to the right: spontaneous emission, where an electron undergoes a transition to a lower energy state and the difference in energy is emitted as a photon.

This description gives a very basic overview of excitation and de-excitation processes. For the purpose of understanding the physical processes present in the topic of this research project, it is necessary to expand this picture and describe the response of a material to an electric field in more detail.

First, the Einstein picture must be expanded to also include the dipole nature of an excitation: if the wavelength of the incident radiation that induces the excitation is larger than the size of the atom, the electrical field can be approximated to be uniform over the atom [11]. Since the nucleus and electron have opposite signs, the field creates a displacement of the electron cloud and an electrical dipole moment is created [12]. This interaction between the atom and the field $\bar{E}$ is commonly described by the electric dipole Hamiltonian:

$$\hat{H}_{dipole} = e\bar{r} \cdot \bar{E}(\bar{r}, t)$$

$$\hat{H}_{dipole} = \mu \bar{E}(\bar{r}, t) \tag{1}$$

where $\bar{r}$ is the position of the electron with regards to the atomic center of mass [10], and μ is introduced to represent the fraction of the dipole moment that is aligned with $\bar{E}$ [12]. From here on, μ will be referred to as the dipole moment.

The dipole can be described in the electron wave function by expressing the displacement as a superposition of two or more electron orbitals [12], as depicted

in Fig. 2 for an s-orbital and a p-orbital. Such a superposition can be expressed as [10]:

$$\Psi(\bar{r},t) = c_1\tilde{\psi}_1(\bar{r},t) + c_2\tilde{\psi}_2(\bar{r},t) \tag{2}$$

where $c_{1,2}$ are constants that describe the strength of the respective component, such that the probability of finding the electron in the eigenstate i is $|c_i|^2$.

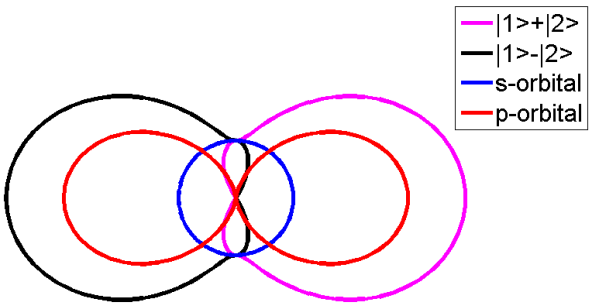

Figure 2: Two-dimensional representation of the probability density of the position of the electron with the nucleus at the origin. The blue line represents an s-orbital and the red line represents a p-orbital. The orbitals are not normalized in order to avoid too much overlap in the figure.

The temporal evolution can be seen more clearly by rewriting Eq. 2 into [10]:

$$\Psi(\bar{r},t) = c_1 e^{-iE_1 t/\hbar}\psi_1(\bar{r}) + c_2 e^{-iE_2 t/\hbar}\psi_2(\bar{r}) \Leftrightarrow$$

$$\Psi(\bar{r},t) = c_1\psi_1(\bar{r}) + c_2 e^{-i(E_1-E_2)t/\hbar}\psi_2(\bar{r}) \tag{3}$$

where E_i is the energy eigenvalue of the state. Here it can be seen that the time dependence of the wave function can be expressed as a phase that relates c_2 to c_1. This phase ϕ is thus given by:

$$\phi = (E_1 - E_2)t/\hbar \tag{4}$$

The time dependence will make sure that the dipole created by the superposition oscillates. To see this, the electron cloud when $c_1 = c_2$, which corresponds to the density cloud called $|1\rangle + |2\rangle$ in Fig. 2, can be compared to the electron cloud when $c_1 = -c_2$, called $|1\rangle - |2\rangle$ in Fig. 2.

The phase of the components is not apparent when only the populations are studied, however it can affect the possibility of transitions to other levels and is therefore an important component for the simulation of a multi-state system interacting with an electromagnetic pulse.

From Eq. 1, it can be seen that the wave nature of the field creates oscillations in the transition frequencies of the system. The transition probability oscillations in turn create oscillations in the populations of the states so that the effect of the field can be seen as moving the population back and forth between the states [11]. The angular frequency of the transition probability oscillations, called the Rabi frequency Ω, is defined as $\Omega = \mu\bar{E}$ [12] and will appear in the simulations later on.

When the energy of the electromagnetic field is not perfectly resonant with the transition, the transition probability between the states will be affected. The detuning δ from the transition frequency, given by $\delta = \omega_{transition} - \omega_{field}$ reduces the probability of a transition. The effect of this could be that the fraction of the the population that is transferred as a consequence of the incident field is reduced.

The final effect that needs to be considered for this research is the Heisenberg uncertainty; when a pulse is very narrow in the time domain, the uncertainty principle gives that the pulse must be broad in the frequency domain [13]. This means that attosecond pulses are very broad in the frequency domain, which is important to the project. This is because the broad frequency range of the attosecond pulses, if correctly tuned, can include several resonant frequencies and thus enables excitation into a mixed state.

3 Method

3.1 Experimental Method

This project is performed in collaboration with the attosecond physics research group at the division of atomic physics at Lund University. The group utilizes a set-up where femtosecond pulses from a Ti:Sapphire laser, with a slightly tunable wavelength of around 800 nm, are used to generate attosecond pulses with wavelengths which are odd harmonics of the tuned laser frequency. Thus by tuning the driving laser, the frequency of the attosecond pulses is also changed [8]. For further details on the manipulation of the pulses and schematic images of the setup at Lund University, see [1].

These attosecond pulses are then incident on a gas chamber where they excite Argon atoms, which then start to oscillate and emit light coherently as they slowly decay to the ground state, which is the energetically lowest state the atom can be in. The emitted light should be identical to the light which initially excited the atom; however in this case the emitted light is steered by a second pulse so that it differs in direction from the initial pulse. The transmitted and emitted light from the gas are then detected with a spectrometer [8]. The time delay between the first pulse and the second is varied to study the effect on the direction of the emitted light - however for this research project the variations in time delay are important for another reason which will be discussed later.

The resulting data from the experiment are in the form of series of spectra, such as the one in Fig. 3c. The specific run that produced the series that is used for this research project was taken by the research group on the 28^{th} of May in 2015, the central frequency of the Ti:Sapphire laser was set to 780 nm and the sampling frequency for the time delay between the pulses was 0.1 fs.

The work carried out for this project starts from the recorded series of spectra, in the form of a matrix with the measured intensities of each pixel. The energy scale of the spectra is along the x-axis, so to find the intensity of each

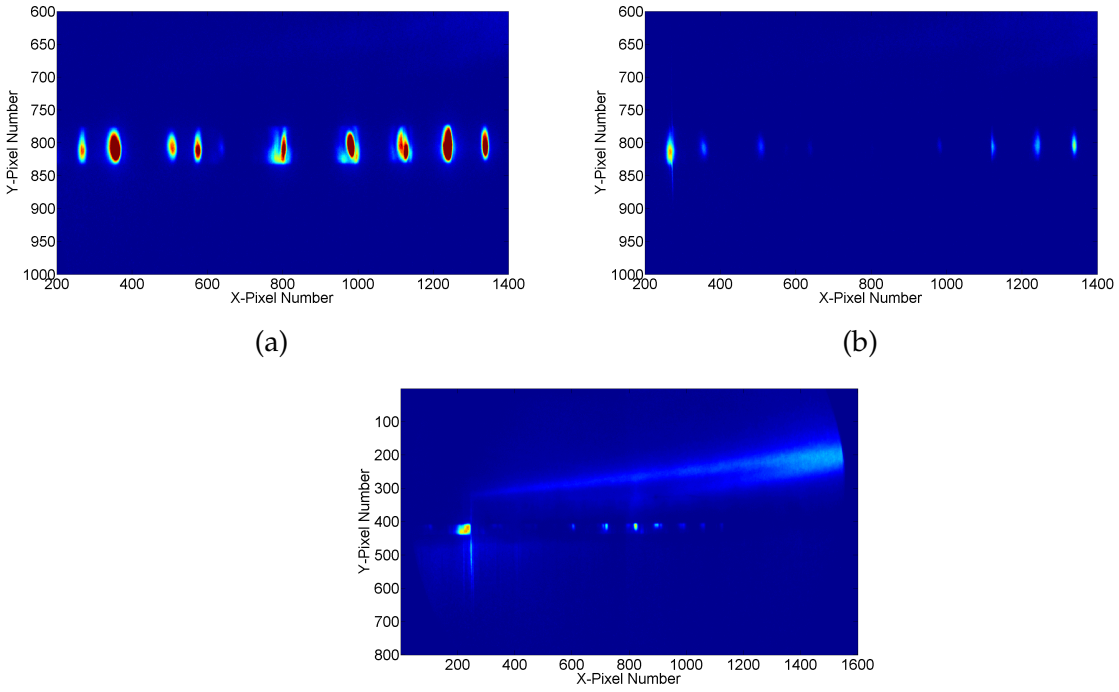

Figure 3: Spectra from the scattering experiment: Image a) shows the attosecond pulses created by high harmonics generation when no Argon gas is present, b) shows the resulting spectrum when Argon gas is present and interacts with the incoming pulses, and finally c) shows the resulting spectrum when Argon gas is present and a second pulse is incident on the Argon atoms a set time after the initial excitation by the attosecond pulse. The longer lines present in this spectrum are the spectral lines whose oscillations are studied in this research project. The axes of the plots indicate the pixels and the color scale indicates the relative intensity of the specified pixel. Image courtesy of the attosecond research group at the division of Atomic Physics at Lund University.

spectral line the total intensity of each row is calculated; in other words, the total intensity of the transition is calculated as the sum of the intensities of all pixels in the column where x corresponds to the transition frequency. The intensity plot is then filtered to reduce noise, and thereafter a sinusoidal function is fitted to the spectrum.

The intensities of the spectrum are proportional to the probability of the transition from the excited state to the ground state; thus by measuring the intensity fluctuations of the spectral lines, information on the probability fluctuations is obtained. The probability of a transition in turn depends on the populations in the levels involved. So by measuring the intensity of spectral lines, information on the populations of the different levels can be extracted.

However, there is a potential problem in simply summing all intensities for one energy value. This is because the resonant pulse that is used to excite the atoms is partially transmitted and the transmitted light appears in the spectrum around and on the transition frequency, thus the intensity

of the transmitted light affects the intensity sum of the transition frequency. When the absorption increases, the transmitted radiation decreases, which affects the intensity sum. However, this problem can be solved by choosing pixels to include in the total intensity sum that are located a few pixels away from the spot where the resonant harmonic hits the spectrometer, since it is only the emitted light that is changed in direction by the second pulse while the transmitted light is not.

3.2 Simulation

Simulations of the multi-state system studied in the experiment described in the previous section was set up in an attempt to reproduce the oscillating pattern seen in the experimental data. First, a two-state system, such as the one described in Fig. 4, was simulated to see if two-state interaction can explain the oscillatory structure of Fig. 7a.

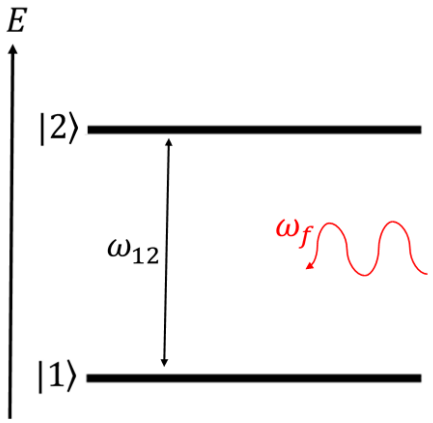

Figure 4: Schematic representation of a two-state system with $|1\rangle$ representing the energetically lower state, and $|2\rangle$ representing the energetically higher state. ω represents the angular frequency of the transition between them and is given by $(E_{upper} - E_{lower})/\hbar$, where ω_f is the angular frequency of the incoming electromagnetic field.

A visually effective way of investigating the relation between the different parameters at play in a two-level system interacting with a field is to use the Bloch notation and the corresponding Bloch sphere. This is done through using the coefficients in the wave function, Eq. 2, to form the following variables [10]:

$$u = c_1 c_2^* e^{-i\delta t} \tag{5a}$$

$$v = -i\left(c_1 c_2^* e^{-i\delta t} - c_2 c_1^* e^{-i\delta t}\right) \tag{5b}$$

$$w = |c_1|^2 - |c_2|^2 \tag{5c}$$

The variables calculated in Eqs. 5 are then used to form the Bloch vector $\bar{R} = (u, v, w)$. By describing the system in this way, different states of the system can be represented as points on a sphere, as shown in Fig. 5. The pure states $|1\rangle$ and $|2\rangle$ are then represented by the vectors $\bar{R} = (0, 0, -1)$ and $\bar{R} = (0, 0, 1)$, respectively.

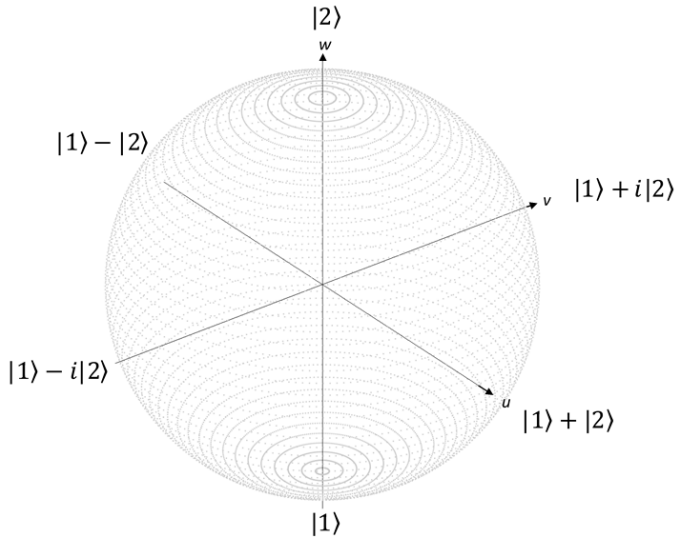

Figure 5: A Bloch sphere which represents a two-state system interacting with an electromagnetic field. The population oscillates between state $|1\rangle$, represented by $R = (0, 0, -1)$, and state $|2\rangle$, represented by $R = (0, 0, 1)$.

The oscillations of the system, described in for example Eq. 3, rotate with a frequency given by Ω. This translates in the Bloch visualization to that Ω controls the rotation of R, or more precisely [12]:

$$\frac{d\bar{R}}{dt} = (Re(\Omega), Im(\Omega), \Delta) \times \bar{R} \tag{6}$$

Eq. 6 is then used to extrapolate the time-dependent values of $\bar{R}$.

The different given parameters that are varied and studied in this system are: the energy difference between the states, the iteration time step, the energy and intensity of the field, the initial state of the electron and the dipole coupling between the field and the two states.

However, the experimental data that are analyzed likely involve at least three states due to the broad frequency range of the pulse, so the project needs additional simulations where this description is expanded to include more states.

The second and third simulations investigate a three-state system where an Argon atom has been excited into a mixed state, containing Argon eigenstates $3s^2 3p^5 5s$ and $3s^2 3p^5 3d$, which then interacts with radiation so that also $3s^2 3p^5 9p$ is included in the electron wave function as described in Fig. 6. The angular momentum quantum numbers of the two lowest states differ by 2, which makes a transition between them first-order forbidden. This is because the angular momentum carried away or added by a photon is ± 1 [10]. The energy values of the states are given in [14] as 113643.260 cm^{-1}, 114147.732 cm^{-1}, and 125039.51 cm^{-1}.

In the first of the three-state simulations the atomic system interacts with two continuous fields and in the second with a laser pulse. Two fields are needed in the first three-state simulation because in the experiment the

pulse is broad in the frequency range, which a field is not, therefore two fields are needed to be able to simulate the effect of an incident light that is resonant with both transitions.

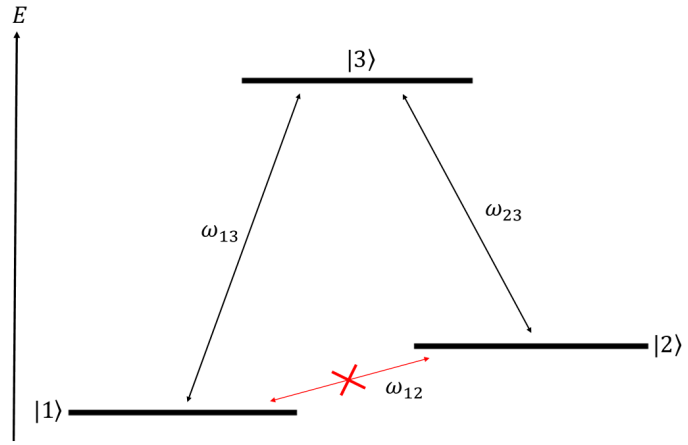

Figure 6: Schematic representation of the three-state system in Argon with $|1\rangle$ representing the state $3s^2 3p^5 5s$, $|2\rangle$ representing the state $3s^2 3p^5 3d$, and $|3\rangle$ representing the state $3s^2 3p^5 9p$. The energy levels of the state are depicted with the energy of the states rising from bottom to top. ω_{ij} represents the angular frequency of a transition between states $|i\rangle$ and $|j\rangle$ and is given by $(E_{upper} - E_{lower})/\hbar$. The transition between state $|1\rangle$ and state $|2\rangle$ is first-order forbidden.

The method in the two-state simulation, calculating the coefficients of the wave function and producing a Bloch sphere, is not practical when three states are included. Instead the density matrix is analyzed. The density matrix is given by [10]:

$$\begin{pmatrix} c_1 \\ c_2 \\ c_3 \end{pmatrix} (c_1^* \; c_2^* \; c_3^*) = \begin{pmatrix} |c_1|^2 & c_1 c_2^* & c_1 c_3^* \\ c_2 c_1^* & |c_2|^2 & c_2 c_3^* \\ c_3 c_1^* & c_3 c_2^* & |c_3|^2 \end{pmatrix} = \begin{pmatrix} \rho_{11} & \rho_{12} & \rho_{13} \\ \rho_{21} & \rho_{22} & \rho_{23} \\ \rho_{31} & \rho_{32} & \rho_{33} \end{pmatrix} \tag{7}$$

The diagonal matrix elements ρ_{ii}, $i = 1, 2$ or 3, are the populations in the respective states. The off-diagonal elements ρ_{ij}, $i \neq j$, describe the couplings for transitions from state i to state j.

The foundation of the simulations is the density matrix derivatives used by Imamoglu [15]. However, unlike in [15], the time scale is here short enough that the states can be considered long-lived, and therefore the probability of spontaneous decay is neglected. When this is taken into account, the time derivatives are found as [15]:

$$\frac{d\rho_{11}}{dt} = \frac{1}{2} i\Omega_{13}(\rho_{31} - \rho_{13}) \tag{8a}$$

$$\frac{d\rho_{22}}{dt} = \frac{1}{2} i\Omega_{23}(\rho_{32} - \rho_{23}) \tag{8b}$$

$$\frac{d\rho_{33}}{dt} = \frac{1}{2}i\Omega_{13}(\rho_{13} - \rho_{31}) + \frac{1}{2}i\Omega_{23}(\rho_{23} - \rho_{32}) \tag{8c}$$

$$\frac{d\rho_{12}}{dt} = -i\Delta\omega_{21}\rho_{12} - \frac{1}{2}i\Omega_{23}\rho_{13} + \frac{1}{2}i\Omega_{13}\rho_{32} \tag{8d}$$

$$\frac{d\rho_{13}}{dt} = i\Delta\omega_{31}\rho_{13} + \frac{1}{2}i\Omega_{13}(\rho_{33} - \rho_{11}) - \frac{1}{2}i\Omega_{23}\rho_{12} \tag{8e}$$

$$\frac{d\rho_{23}}{dt} = i(\Delta\omega_{31} - \Delta\omega_{21})\rho_{23} + \frac{1}{2}i\Omega_{23}(\rho_{33} - \rho_{22}) - \frac{1}{2}i\Omega_{13}\rho_{21} \tag{8f}$$

where Ω_{ij} is the Rabi frequency of a transition between states i and j, and $\Delta\omega_{ij}$ is the detuning between the frequency of the fields, or for the last simulation the central frequency of the pulse, and the frequency difference between states i and j. Eqs. 8 are used in the simulations to extrapolate the temporal evolution of the density matrix.

Since these simulations are based on an existing atomic system, the energy and dipole moments of the states are fixed. The energies of the states from [14] are used together with a dipole moment of $2.0378 \cdot 10^{-29}$ Cm for a transition between states $|1\rangle$ and $|3\rangle$, and a dipole moment of $1.7137 \cdot 10^{-29}$ Cm for a transition between states $|2\rangle$ and $|3\rangle$. The parameters which are varied are solely properties of the field or pulse, and properties of the numerical calculation: for the first simulation the energy and intensity of the fields are varied, as is the iteration step size. For the second simulation the energy, area, delay and width of the pulse are varied, as well as the iteration step size.

4 Results and Discussion

The relation between the delay time and the total intensity of the pixel columns corresponding to the spectral lines of transitions from $3s^2 3p^5 5s$ and $3s^2 3p^5 3d$ to the ground state is shown in Fig. 7a together with a fitted oscillation. It was not expected that the frequencies of the intensity variations of the two spectral lines would differ from each other the way Fig. 7b implies, since the periodicity of the unperturbed population oscillations is given by the phase between c_1 and c_2, and the same periodicity was expected to be found also in the population oscillations depending on the delay time; this since the initial values of c_1 and c_2 are the only variables of importance that were assumed to change depending on the delay time.

The frequencies of the fitted oscillations are found to be 11.9 THz and 13.5 THz. These values are found from fitting a sinusoidal function to the final part of the spectrum, where the system is assumed to have stabilized. The expected frequency is $(E_2 - E_1)/h$, which is found to be 15.1 THz using the energy values given in [14]. The energy difference between state $|1\rangle$ and state $|2\rangle$ which follows from the experimentally produced frequencies is either 49 meV or 56 meV, while the published value is 63 meV.

The frequency discrepancy can be significantly decreased by choosing from which pixels the intensities should be evaluated; by restricting the

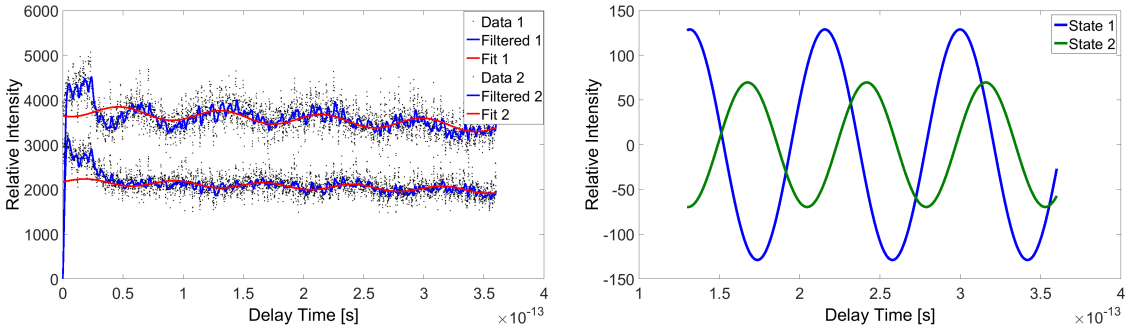

(a) (b)

Figure 7: Temporal evolution of spectral line intensity for Argon, which was calculated from series of spectra such as the one in Fig. 3c, and a fitted oscillation shown as a red line in a) and without the data points in b). The absolute values of the residuals of the fits had a mean value of 90 for the upper line, line 1, and 53 for the lower line, line 2.

analysis to pixels which are unaffected by the intensity of the transmitted pulse, two oscillations of the same frequency can be deduced from the series of spectra as seen in Fig. 7. However, the intensities of the spectral lines are not as prominent further away from the spot where the resonant harmonic hits the spectrometer, so the signal is weaker in these parts of the spectra.

The frequency which is found from Fig. 8 is 13.0 THz, which corresponds to an energy difference between state $|1\rangle$ and state $|2\rangle$ of 54 meV. The difference between this value and the published value could be due to Stark shifting; this is a shift of the energy levels of the electron states when the atom interacts with an electric field. The shift decreases the energy splitting between the states for a positive frequency detuning [10], which probably is the case for this experimental work.

The first thing which was apparent when the first simulation was run was the importance of tuning the iteration time step dt to be small enough. For a dt which is too large, the Bloch sphere grows to infinity. This is of course not physically possible since a probability of finding the electron in a certain state cannot be higher than 1. The frequency of the field plays a part in tuning dt: the larger detuning from the transition frequency, the quicker the system oscillates and the smaller dt is needed in order not to miss any part of the oscillations which usually leads to an infinite growth of the system in the simulation. Another parameter that was seen to cause non-physical growth of the system is to increase the dipole moment; since the Rabi frequency is proportional to the dipole moment, the size of the dipole moment affects how fast the system is evolving and thus also affects how small dt needs to be. A high field intensity also demands a small dt, which is to be expected; the frequency of the oscillations is also proportional to the intensity of the field. Should the intensity be too low, there are simply no oscillations and the system stays in its initial state.

In Fig. 9, the effect of introducing a non-zero detuning can be seen as

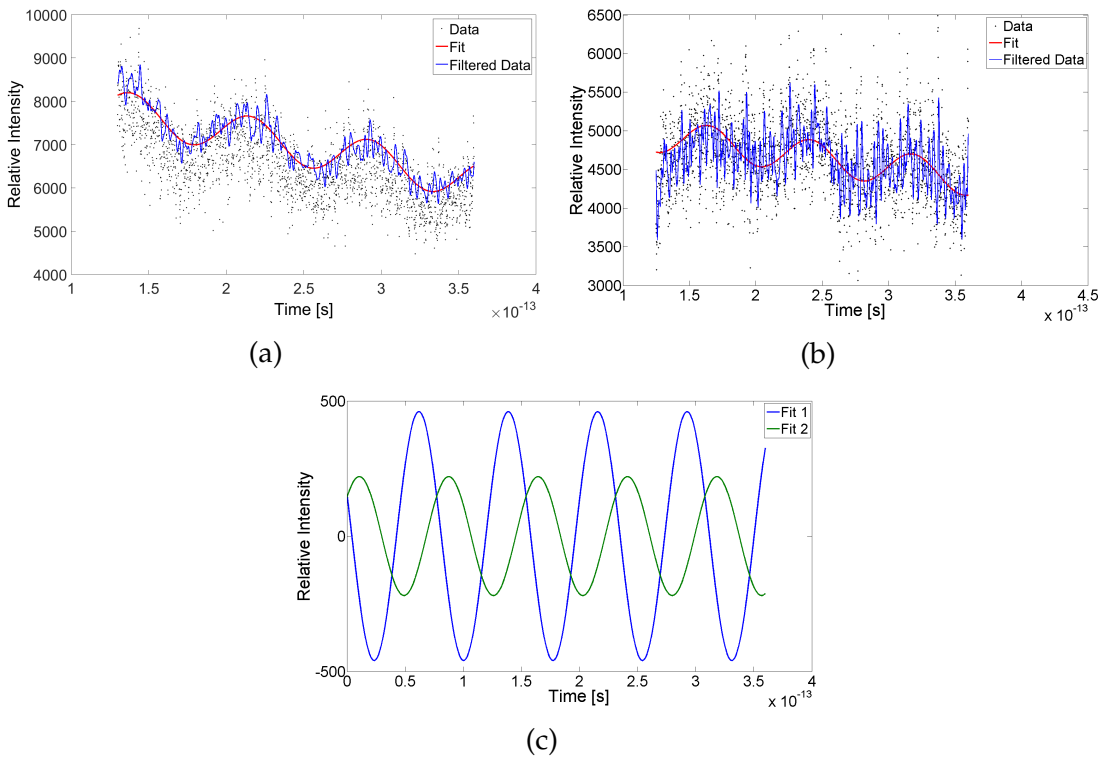

Figure 8: Intensities of the spectral lines that were calculated from pixels of the initial series of spectra, which are chosen specifically because they are largely unaffected by the intensity of the transmitted pulse. The blue lines show the result when a low pass filter has been applied to the data. The red line shows fitted oscillations with a frequency of 13.0 THz, corresponding to an energy splitting of 54 meV between the states. In c), only the fits are shown. The absolute value of the residuals of the fits had an average value of 191 for line 1 and 370 for line 2.

a decrease in the size of the w-component. This can be seen in the vector representation as an inclination of the plane in which the vector rotates, which causes the cut-offs in the w-direction seen in Fig. 9d. By comparing Fig. 9a and 9b, it can also be seen that the period of the oscillation is shorter when a non-zero detuning is introduced. The initial state of the system is important; when the initial value of the u-component is non-zero, the oscillations in the w-component will be reduced. However, even for an initial state $R = (\pm 1, 0, 0)$, there are still oscillations in the w-component albeit very small. Any initial state with the u-component set to zero results in oscillations of the w-component between 1 and -1, which corresponds to that the entire population is moved from state $|1\rangle$ to state $|2\rangle$.

If the oscillations in Fig. 7 would have been the result of two-state interaction, the expected fitted functions would be in the form of two sinusoidal waves where a crest of the intensity of one spectral line occurs at the same time as a trough of the other line. This can be seen from Fig. 9, in the even oscillations of the w-component: when the vector has its maximum fraction of state $|1\rangle$, state $|2\rangle$ has its minimum. However, from the experimental re-

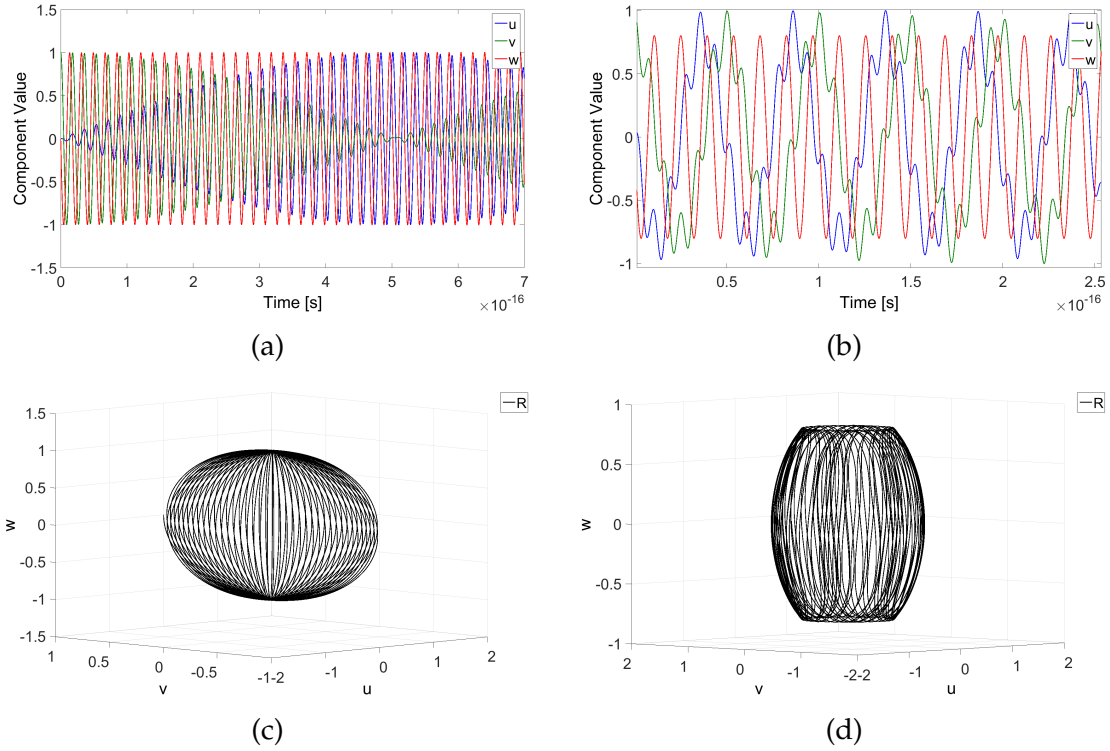

Figure 9: Simulation results from running the simulation of a two-state atomic system interacting with a laser field, with the initial Bloch state $R = (0, 1, 0)$. In a) and b), the temporal evolution of the three components of the Bloch vector is presented. For a), the field is resonant with the transition. In b), the field is detuned from the resonance frequency. In c) and d) the Bloch sphere representation is shown, with each line corresponding to the Bloch vector at a specific time. In c), the field is resonant. In d), the frequency of the field is detuned from the transition frequency.

sult in Fig. 8c, it can be seen that the troughs of one line are displaced temporally from the crests of the other line and vice versa; thus a two-state system does not seem sufficient to explain the oscillations in the spectral line intensity.

The results from running the three-state system simulation show that also here the size of dt is important in the same way as for the two-state system; if the field frequency or intensity are increased without proper decrease of dt, the system grows unrealistically large. The temporal evolution of the system is shown in Fig. 10, and from the figures it can be seen that dt is larger than what it should ideally be; however, a smaller dt was not possible to use due to limits in the accessible computational power. The effect of introducing a detuning can be seen by comparing Fig. 10a and 10b, which show the same differences as the previous simulation; the amplitude of the population oscillations is decreased when a detuning is introduced and the period of the oscillations decreases. The effect of changing the initial state to being completely in state $|1\rangle$ is shown in Fig. 10c, and can be seen as a decrease in the amplitude of the oscillations but the period of the oscillations

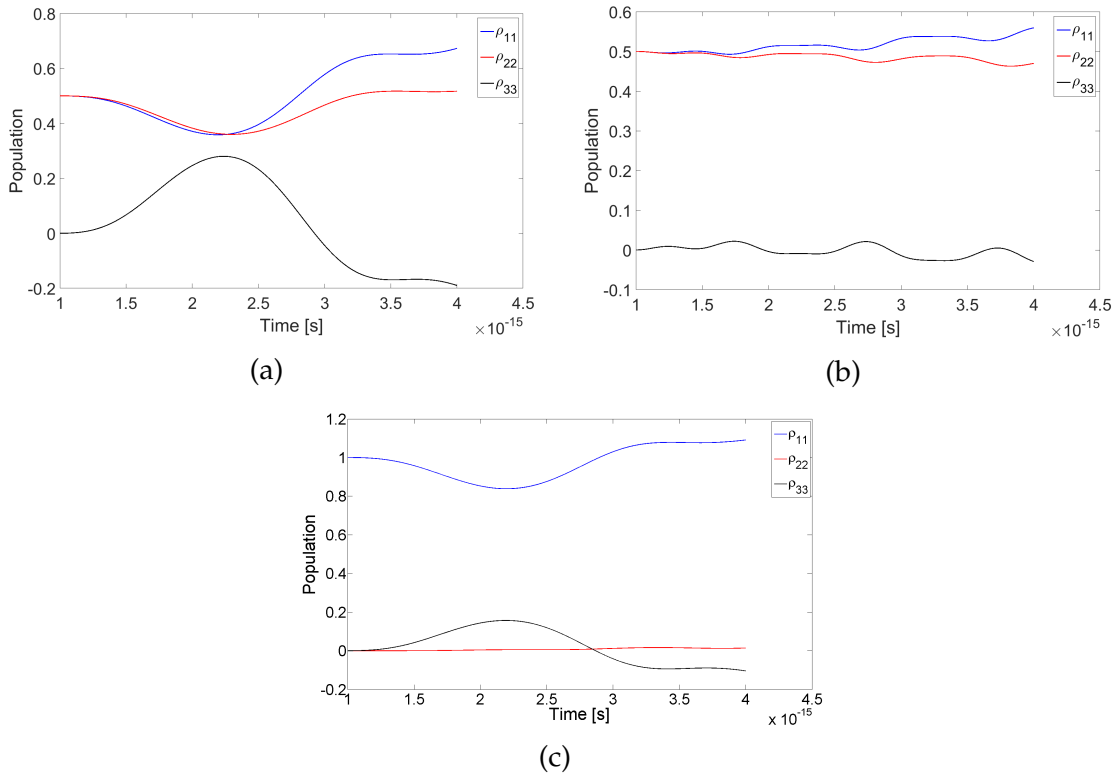

Figure 10: Simulation results from running the simulation of a three-state atomic system interacting with a laser field. In a), the temporal evolution of the system interacting with resonant fields is presented. The initial state of the electron for this plot is $c_1 = c_2 = \sqrt{\frac{1}{2}}$. In b), the plot shows the evolution of the same system with the same initial state of the electron but here the frequencies of the fields are detuned from the transition frequencies. In c), the effect of changing the initial state to $c_1 = 1$ is shown for resonant fields.

remains the same as in Fig. 10a where the initial state is a superposition of state $|1\rangle$ and $|2\rangle$. Changing the initial state to being fully in state $|2\rangle$ results in a plot that is very similar to 10c. If the initial state is set to a superposition in the form of $|1\rangle - |2\rangle$, with equal magnitude of c_1 and c_2, the oscillations are heavily damped but the period is unchanged. This dependence on the composition of the superposition state is not completely unexpected; it is known that certain compositions of electron superposition states can give rise to so called "dark states" where transitions are inhibited [11].

When the continuous fields are replaced with a pulse, two additional parameters are introduced to the system: the width of the pulse and the delay between the initial creation of the system (in the actual experiment this is the time of the excitation into the coherently excited state containing $3s^2 3p^5 5s$ and $3s^2 3p^5 3d$), and the time when the pulse is incident on the system. Also, the intensity of the field is replaced with the area of the pulse. The evolution of the three-state system interacting with a pulse is presented in Fig. 11a.

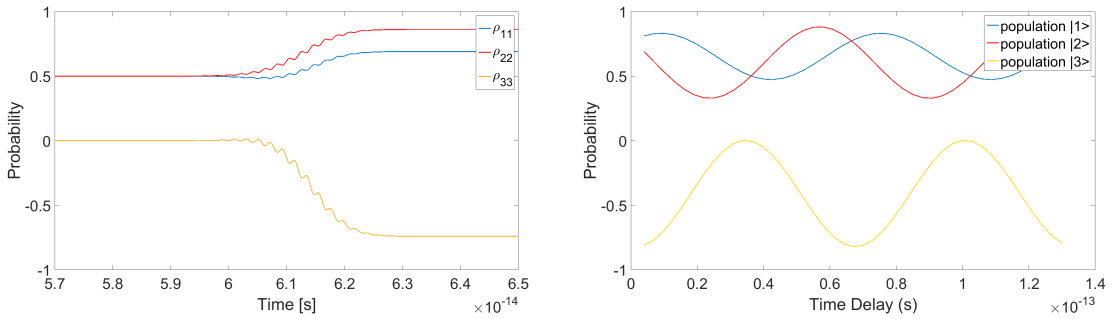

(a) (b)

Figure 11: Results of the simulation where a three-state system interacts with a pulsed electric field. a) shows an example of the temporal evolution of the population, where the different lines represent the population in the different states. b) shows the final state of the excited electron as a function of the time delay between the initial excitation into the three-state system and the second pulse.

Once again, it is clear that the appropriate size of the iteration time step is highly sensitive to changes in the parameters which affect the frequency of the oscillations. The simulation responds to changes in the area of the pulse in the same way as the continuous-fields three-state system responds to changes in the intensity of the fields. The growth of the system is seen clearly in Fig. 11 since the probability of finding an electron in state $|3\rangle$ frequently is below zero in the plots, which is physically unreasonable. Although, even without the growth there seems to exist oscillations in the population of state $|3\rangle$, since there are peaks which are clearly above zero if the plot is zoomed in on the oscillations of the third state. There is another factor that implies that the results have some significance despite this growth: The population oscillations of state $|1\rangle$ and state $|2\rangle$, seen in Fig. 11b, have approximately the same period of about 65 fs, which gives an energy splitting of 63 meV - this coincides with the difference between state $|1\rangle$ and state $|2\rangle$. Thus the overall pattern seem to imply that the simulation works as intended, except for the growth.

If the overall pattern of the simulation is correct, the simulated population oscillations of state $|1\rangle$ and state $|2\rangle$ look very similar to the fitted functions to the experimental result from Fig. 8c, as shown in Fig. 12. Thus the simulation seem to imply that the oscillating pattern in the spectral line intensity indeed can be explained by the inclusion of a third, higher lying state in the mixed excited state as a consequence of the second pulse. This means that a certain amount of control should be possible to exert on the composition of the stabilized superposition of the electron by varying the delay between the pulses.

However, it is worth mentioning that the results of the project do not give any indications as to which state $|3\rangle$ represents; the only effect a change of state $|3\rangle$ from $3s^2 3p^5 9p$ to another state would have on the results is in the temporal evolution of the coherently excited state, provided that the

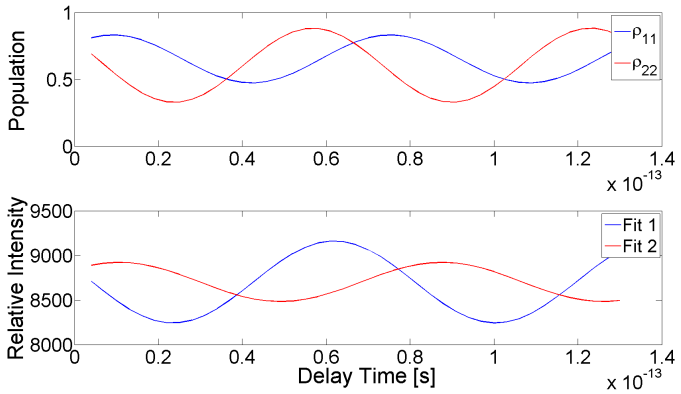

Figure 12: Top plot: The population oscillations of state $|1\rangle$ and state $|2\rangle$, obtained from the simulation. Lower plot: The fitted functions of the intensity oscillations of the spectral lines for transitions from state $|1\rangle$ and $|2\rangle$, respectively.

new $|3\rangle$ is not too far different from $3s^2 3p^5 9p$ in energy. The obstacle is that the temporal evolutions, such as the one in Fig. 11a, are not detected in the experiment - except for the stabilized final state. The period of the population oscillations of state $|1\rangle$ and $|2\rangle$ in Fig. 11 is not expected to change if the upper state is changed, because the period depends on the periodicity of the two-state superposition that evolves before the second pulse is incident on the system.

As for the identification of the two lower states, the experimental result for the energy splitting between state $|1\rangle$ and state $|2\rangle$ found from Fig. 8 of 54 meV coincides well enough with the published value of 63 meV, especially if the possible effect of a Stark shift is considered, that it seems probable that these spectral lines indeed correspond to the states $3s^2 3p^5 5s$ and $3s^2 3p^5 3d$.

5 Outlook

If a project such as this one is to be undertaken again, the method of extrapolation should be improved; mainly to address the problem of the growing amplitude for example in Fig. 10, but also to save computational power and through this enable a higher number of simulations. One suggestion for a better way of extrapolating would be to discard the simple method used in this project, where a point $P(i+1)$ is found by using the derivative in the previous point:

$$P(i+1) = P(i) + P'(i) \cdot dt \tag{9}$$

as in the first two simulations, or by also using the derivative in the previous point and the derivative in a point between the previous and the current point, as stated in Heun's method [16], which is partly introduced in the third simulation. It would probably be beneficial to use a slightly more advanced method instead, for example an implicit method where an initial

guess is first used and then corrected by using derivatives from points both before and after the current iteration point [16].

The next improvement which could be made is to include effects of the Stark shift, which was initially neglected because it has previously been assumed that when a pulse is narrow in the time domain it does not have a considerable impact on the energy levels [17]. However, the energy splitting between the states which is found from the experimental data is slightly smaller than the expected one and therefore the effect of the Stark shift may be more important than initially assumed and it should probably not be neglected.

Another issue which could be addressed is the nature of the pulse: in the simulations performed in this project, the pulses have been assumed to be Gaussian. This assumption has previously been thought of as a possible source of discrepancy between experimentally produced results and simulations [9], and seems like a possible source also in this case.

One of the first assumptions made, that the excited atom can be modeled as a three-state system, is undoubtedly a simplification; close-lying states interfering is probable and might also affect the oscillations in Fig. 7a and 7b; if there are other states involved, this changes the angular frequency of the oscillations so that it is no longer given by $(E_2 - E_1 / \hbar)$.

If the third state is to be identified, the method needs to be expanded to either include additional experimental measurements, for example an improved simulation could yield clues as to how the intensity of the spectral line of the third state should vary and this line could then be searched for in the spectra. In this case, the frequency of the transition from the third state to the ground state needs to be a certain distance away from the odd harmonics of the driving laser in order not to be hidden in the transmitted light, unless a way is found to deflect the transmitted light.

Another, likely more manageable, suggestion is to analyze the displacement of the population troughs of state $|1\rangle$ compared to the crests of state $|2\rangle$ since this is seems to be the only feature that is detectable experimentally where the third state has any influence on the outcome. If the simulation is improved so that the growth issue is addressed, it might be possible to run the simulation for a few different states as the third state and see whether a match can be made between the displacement created in the simulation and the displacement found experimentally.

A final suggestion as to how the third state could be identified is to use a set delay time between the first and the second pulse and then use an additional pulse, which is incident on the system a tunable time after the second pulse. Perhaps it would then be possible to extract the period of the temporal evolution of the three-state superposition by varying the time delay between the second and third pulse and study the frequency of the spectral line oscillations to gain information about the energy splitting to the third state compared to the other states, in the same way the time delay between the first and the second pulse is varied to find the energy splitting between state $|1\rangle$ and state $|2\rangle$ in this project. If the energy splitting can

be found, the third state should be able to find from the energy values of $3s^2 3p^5 5s$ and $3s^2 3p^5 3d$.

In short, the results and conclusions drawn from the project are mainly that it seems as though the experimentally observed intensity fluctuations of the spectral lines can indeed be explained fairly well by three-state interaction, however the identification of the third state remains unclear. Also, a certain amount of control should be possible to exert on the composition of the stabilized superposition after the second pulse by varying the time delay between the first and the second pulse.

Projects and studies on this topic are of major importance for the prospect of being able to steer the electron dynamics on a timescale where no major cooling of the electron to slow down the dynamics is needed. If this particular area of research is successful, it seems likely that a number of new technological and scientific advances will follow in its wake.

References

[1] D. Kroon, *Attosecond interferometry: techniques and spectroscopy*. PhD thesis, Lund University, 2016.

[2] O. Pedatzur, G. Orenstein, H. Soifer, B. Bruner, A. Uzan, O. Smirnova, N. Dudovich, V. Serbinenko, D. Brambila, A. Harvey, L. Torlina, and F. Morales, "Attosecond tunnelling interferometry.," *Nature Physics*, vol. 11, no. 10, pp. 815–819, 2015.

[3] F. Kärtner, F. Ahr, A.-L. Calendron, H. Çankaya, S. Carbajo, G. Chang, G. Cirmi, K. Dörner, U. Dorda, A. Fallahi, A. Hartin, M. Hemmer, R. Hobbs, Y. Hua, W. Huang, R. Letrun, N. Matlis, V. Mazalova, O. Mücke, E. Nanni, W. Putnam, K. Ravi, F. Reichert, I. Sarrou, X. Wu, A. Yahaghi, H. Ye, L. Zapata, D. Zhang, C. Zhou, R. Miller, K. Berggren, H. Graafsma, A. Meents, R. Assmann, H. Chapman, and P. Fromme, "Axsis: Exploring the frontiers in attosecond x-ray science, imaging and spectroscopy," *Nuclear Instruments and Methods in Physics Research Section A: Accelerators, Spectrometers, Detectors and Associated Equipment*, 2016.

[4] A. Mikkelsen, J. Schwenke, T. Fordell, G. Luo, K. Klünder, E. Hilner, N. Anttu, A. Zakharov, E. Lundgren, J. Mauritsson, J. N. Andersen, H. Xu, and A. L'Huillier, "Photoemission electron microscopy using extreme ultraviolet attosecond pulse trains," *Review of Scientific Instruments*, vol. 80, no. 12, 2009.

[5] E. Mårsell, C. Arnold, E. Lorek, D. Guenot, T. Fordell, M. Miranda, J. Mauritsson, H. Xu, A. L'Huillier, and A. Mikkelsen, "Secondary electron imaging of nanostructures using extreme ultra-violet attosecond pulse trains and infra-red femtosecond pulses," *Annalen der Physik*, vol. 525, no. 1-2, pp. 162–170, 2013.

[6] M. Swoboda, T. Fordell, K. Klünder, J. M. Dahlström, M. Miranda, C. Buth, K. J. Schafer, J. Mauritsson, A. L'Huillier, and M. Gisselbrecht, "Phase measurement of resonant two-photon ionization in helium," *Phys. Rev. Lett.*, vol. 104, p. 103003, Mar 2010.

[7] M. Kotur, D. Guénot, D. Kroon, E. Larsen, M. Louisy, S. Bengtsson, M. Miranda, J. Mauritsson, C. Arnold, M. Gisselbrecht, A. L'Huillier, A. Jiménez-Galán, L. Argenti, F. Martín, S. Canton, T. Carette, J. Dahlström, E. Lindroth, and A. Maquet, "Spectral phase measurement of a fano resonance using tunable attosecond pulses.," *Nature Communications*, vol. 7, 2016.

[8] E. Larsen, S. Bengtsson, D. Kroon, C. Arnold, A. L'Huillier, L. Rippe, and J. Mauritsson, "Controlling free induction decay using strong fields and xuv pulses," *manuscript in production*.

[9] W. Cao, E. Warrick, D. Neumark, and S. Leone, "Attosecond transient absorption of argon atoms in the vacuum ultraviolet region:

Line energy shifts versus coherent population transfer.," *New Journal of Physics*, vol. 18, no. 1, 2016.

[10] C. Foot, *Atomic Physics*. Oxford Master Series in Physics, OUP Oxford, 2004.

[11] C. Gerry and P. Knight, *Introductory Quantum Optics*. Cambridge University Press, 2005.

[12] L. Rippe, *Quantum computing with naturally trapped sub-nanometre-spaced ions*. PhD thesis, Lund University, 2006.

[13] S. McMurry, *Quantum Mechanics*. Pearson Education, Addison-Wesley, 1993.

[14] A. Kramida, Y. Ralchenko, J. Reader, and and NIST ASD Team. NIST Atomic Spectra Database (ver. 5.3), [Online]. Available: `http://physics.nist.gov/asd` [2016, April 27]. National Institute of Standards and Technology, Gaithersburg, MD., 2015.

[15] A. Imamolu, J. E. Field, and S. E. Harris, "Lasers without inversion: A closed lifetime broadened system," *Phys. Rev. Lett.*, vol. 66, pp. 1154–1156, Mar 1991.

[16] M. T. Heath, *Scientific Computing: An Introductory Survey*. McGraw-Hill Higher Education, 2nd ed., 1996.

[17] C. Ott, A. Kaldun, P. Raith, K. Meyer, M. Laux, J. Evers, C. H. Keitel, C. H. Greene, and T. Pfeifer, "Lorentz meets fano in spectral line shapes: A universal phase and its laser control," *Science*, vol. 340, no. 6133, pp. 716–720, 2013.

Appendices

A Simulation of a Three-State System Interacting with a Laser Pulse

A.1 Start Program

```
clear all

h = 6.626070040*10^(-34);
hb = 1.0545718*10^(-34);
hc = 1.98644568*10^(-25);
e = 1.60217662*10^(-19);
c = hc/h;

dt = 10^(-21);              % Optimize computational speed/growth
tf = 13.5*10^(-14);
t_0 = 0;
t = transpose(t_0:dt:tf);

w1 = 14.08998*e/h;           % from Nist for 5s j=1
w2 = 14.1525*e/h;               % from Nist for 3d j=1
w3 = 15.50293*e/h;            % from Nist for 9p j=1
lambda_l = 780*10^(-9);        % Wavelength of the driving laser
wc = 2*pi*c/lambda_l;
energies = [w1 w2 w3 wc];

d31 = 2.0378*10^(-29);          % Dipole moments
d32 = 1.7137*10^(-29);

% Pulse properties
pulse_width = 2*10^(-15);
pulse_area = 5*pulse_width*10^10;
phi = pi/4;
d_delay = 3*10^(-15);
delays = [(pulse_width*2):d_delay:13.24*10^(-14)];
if delays(length(delays))>= tf;
    disp('t_f too small')
    break
end

% Setting initial state of the electron
c1 = sqrt(1/2);
c2 = sqrt(1/2);
c3 = 0;

initial_values = [c1 c2 c3];

for index = 1:1:length(delays);
    dummy_t = transp(delays(index)-pulse_width*2:dt:delays(index)+pulse_width*2);

% Creating the pulse
central_t = delays(index);
A = Gauss2(pulse_area,central_t, pulse_width,dummy_t);
E = A.*exp(-1i*(2*pi*wc.*dummy_t+phi));

% Defining the Rabi frequencies
Om13 = -d31.*E./(2.*hb);
Om23 = -d32.*E./(2.*hb);
Rabis = [Om13 Om23];

% Temporal evolution for the current Delay Time
d_M = d_matrix_evol_gp(initial_values,t,Rabis,energies,delays(index),pulse_width);

[frames rows columns] = size(d_M);
```

```
final_pop(index,1) = d_M(frames-1,1,1);
final_pop(index,2) = d_M(frames-1,2,2);
final_pop(index,3) = d_M(frames-1,3,3);

% To check the evolution of the initial state depending on the delay
init_st(index,1)=  d_M(1,4,1);
init_st(index,2)=  d_M(1,4,2);
init_st(index,3)=  d_M(1,4,3);

% Plotting every tenth evolution
if  index/10 - floor(index/10) == 0;
    figure
    plot(dummy_t(1:length(dummy_t)-1),d_M(:,1,1), dummy_t(1:length(dummy_t)-1),d_M(:,2,2),
    dummy_t(1:length(dummy_t)-1),d_M(:,3,3));
    legend({'\rho_{11}','\rho_{22}','\rho_{33}'},'FontSize',24)
    xlabel({'Time [s]'},'FontSize',24)
    ylabel({'Probability'},'FontSize',24)
    title({['Time Delay for pulse: ' num2str(delays(index)),' s']},'FontSize',24)
end

end

% Plotting the delay dependence
figure
plot(delays,final_pop(:,1),delays,final_pop(:,2),delays,final_pop(:,3))
legend({'population |1>','population |2>','population |3>'},'FontSize',24)
xlabel({'Time Delay (s)'},'FontSize',24)
ylabel({'Probability'},'FontSize',24)
```

A.2 Creating the Pulse

```
function G = Gauss2(peak_area, central_x, FWHM,x)
G = 2/(FWHM*sqrt(pi/log(2))).*exp(-4*log(2).*(x-central_x).^2./(FWHM^2)).*peak_area;
```

A.3 Temporal Evolution

```
function d_M = d_matrix_evol_gp(initial_values,t,Rabis, energies, delay,pulse_width)
% Heun's method of extrapolation

h = 6.626070040*10^(-34);
hb = 1.0545718*10^(-34);
hc = 1.98644568*10^(-25);
e = 1.60217662*10^(-19);
c = hc/h;

dt = t(2)-t(1);
t_t = delay-pulse_width*2:dt:delay+pulse_width*2;

w1 = energies(1);
w2 = energies(2);
w3 = energies(3);
wc = energies(4);

% Setting rotating frame frequency
wp = w3-w1;

% Taking the temporal evolution before the pulse into account
c1 = initial_values(1)*exp(-1i*w1*2*pi*t_t(1));
c2 = initial_values(2)*exp(-1i*w2*2*pi*t_t(1));
c3 = initial_values(3)*exp(-1i*w3*2*pi*t_t(1));

Om13 = Rabis(:,1);
Om23 = Rabis(:,2);

% Defining the detunings
Delw21 = w2-w1;
Delw31 = w3-w1-wc;
```

```
% Pre-allocating for speed
p11 = zeros(length(t_t)-2,1);
p22 = zeros(length(t_t)-2,1);
p33 = zeros(length(t_t)-2,1);
p12 = zeros(length(t_t)-2,1);
p21 = zeros(length(t_t)-2,1);
p13 = zeros(length(t_t)-2,1);
p31 = zeros(length(t_t)-2,1);
p23 = zeros(length(t_t)-2,1);
p32 = zeros(length(t_t)-2,1);

dp11_dt = zeros(length(t_t),1);
dp22_dt = zeros(length(t_t),1);
dp33_dt = zeros(length(t_t),1);
dp12_dt = zeros(length(t_t),1);
dp13_dt = zeros(length(t_t),1);
dp23_dt = zeros(length(t_t),1);

k2_11 = zeros(length(t_t),1);
k2_22 = zeros(length(t_t),1);
k2_33 = zeros(length(t_t),1);
k2_12 = zeros(length(t_t),1);
k2_13 = zeros(length(t_t),1);
k2_23 = zeros(length(t_t),1);

% Defining initial density matrix and derivatives
p11(1) = abs(c1)^2;
p22(1) = abs(c2)^2;
p33(1) = abs(c3)^2;
p12(1) = c1*conj(c2);
p21(1) = c2*conj(c1);
p13(1) = c1*conj(c3);
p31(1) = c3*conj(c1);
p23(1) = c2*conj(c3);
p32(1) = c3*conj(c2);

dp11_dt(1) = 1/2.*1i*Om13(1)*(p31(1)-p13(1));
dp22_dt(1) = 1/2*1i*Om23(1)*(p32(1)-p23(1));
dp33_dt(1) = 1/2*1i*Om13(1)*(p13(1)-p31(1)) + 1/2*1i*Om23(1)*(p23(1)-p32(1));
dp12_dt(1) = 1i*Delw21*p12(1) - 1/2*1i*Om23(1)*p13(1) + 1/2*1i*Om13(1)*p32(1);
dp13_dt(1) = 1i*Delw31*p13(1) + 1/2*1i*Om13(1)*(p33(1)-p11(1)) - 1/2*1i*Om23(1)*p12(1);
dp23_dt(1) = 1i*(Delw31-Delw21)*p23(1) + 1/2*1i*Om23(1)*(p33(1)-p22(1))
-1/2*1i*Om13(1)*p21(1);

% Derivative in point halfway between first and second iteration point
k2_11(1) = 1/2.*1i*(Om13(1)-Om13(2))/2
*(p31(1)+conj(dt*dp13_dt(1)/2)-p13(1)-dt*dp13_dt(1)/2);
k2_22(1) = 1/2*1i*(Om23(1)+Om23(2))/2*
(p32(1)+ conj(dt*dp23_dt(1)/2)- p23(1)-(dt*dp23_dt(1)/2));
k2_33(1) = 1/2*1i*(Om13(1)+Om13(2))/2*
(p13(1)+(dt*dp13_dt(1)/2)-p31(1)-conj(dt*dp13_dt(1)/2))
 + 1/2*1i*(Om23(1)+Om23(2))/2*(p23(1)+(dt*dp23_dt(1)/2)-p32(1)-conj(dt*dp23_dt(1)/2));
k2_12(1) = 1i*Delw21*(p12(1)+(dt*dp12_dt(1)/2)) -
1/2*1i*(Om23(1)+Om23(2))/2*(p13(1)+(dt*dp13_dt(1)/2))
 + 1/2*1i*(Om13(1)+Om13(2))/2*(p32(1)+(dt*dp23_dt(1)/2));
k2_13(1) = 1i*Delw31*(p13(1)+(dt*dp13_dt(1)/2)) +
 1/2*1i*(Om13(1)+Om13(2))/2*(p33(1)+(dt*dp33_dt(1)/2)-p11(1)-(dt*dp11_dt(1)/2))
- 1/2*1i*(Om23(1)+Om23(2))/2*(p12(1)+(dt*dp12_dt(1)/2));
k2_23(1) = 1i*(Delw31-Delw21)*(p23(1)+(dt*dp23_dt(1)/2))
+ 1/2*1i*(Om23(1)+Om23(2))/2*(p33(1)+(dt*dp33_dt(1)/2)-p22(1)-(dt*dp22_dt(1)/2))
-1/2*1i*(Om13(1)+Om13(2))/2*(p21(1)+conj(dt*dp12_dt(1)/2));

% Temporal evolution of density matrix
for index = 1:length(t_t)-2;

    p11(index+1) = p11(index)+(k2_11(index)+dp11_dt(index))*dt/2;
    p22(index+1) = p22(index)+(k2_22(index)+dp22_dt(index))*dt/2;
    p33(index+1) = p33(index)+(k2_33(index)+dp33_dt(index))*dt/2;
    p12(index+1) = p12(index)+(k2_12(index)+dp12_dt(index))*dt/2;
    p21(index+1) = conj(p12(index+1));
```

```
    p13(index+1) = p13(index)+(k2_13(index)+dp13_dt(index))*dt/2;
    p31(index+1) = conj(p13(index+1));
    p23(index+1) = p23(index)+(k2_23(index)+dp23_dt(index))*dt/2;
    p32(index+1) =  conj(p23(index+1));

    dp11_dt(index+1) = 1/2.*1i*Om13(index+1)*(p31(index+1)-p13(index+1));
    dp22_dt(index+1) = 1/2*1i*Om23(index+1)*(p32(index+1)-p23(index+1));
    dp33_dt(index+1) = 1/2*1i*Om13(index+1)*(p13(index+1)-p31(index+1))
+ 1/2*1i*Om23(index+1)*(p23(index+1)-p32(index+1));
    dp12_dt(index+1) = 1i*Delw21*p12(index+1) - 1/2*1i*Om23(index+1)*p13(index+1)
 + 1/2*1i*Om13(index+1)*p32(index+1);
    dp13_dt(index+1) = 1i*Delw31*p13(index+1)
+ 1/2*1i*Om13(index+1)*(p33(index+1)-p11(index+1))
 - 1/2*1i*Om23(index+1)*p12(index+1);
    dp23_dt(index+1) = 1i*(Delw31-Delw21)*p23(index+1)
+ 1/2*1i*Om23(index+1)*(p33(index+1)-p22(index+1))
-1/2*1i*Om13(index+1)*p21(index+1);

    k2_11(index+1) = 1/2.*1i*(Om13(index+1)-Om13(index+2))/2
*(p31(index+1)+conj(dt*dp13_dt(index+1)/2)-p13(index+1)-dt*dp13_dt(index+1)/2);
    k2_22(index+1) = 1/2*1i*(Om23(index+1)+Om23(index+2))/2
*(p32(index+1)+ conj(dt*dp23_dt(index+1)/2) - p23(index+1)-(dt*dp23_dt(index+1)/2));
    k2_33(index+1) = 1/2*1i*(Om13(index+1)+Om13(index+2))/2*
(p13(index+1)+(dt*dp13_dt(index+1)/2)-p31(index+1)-conj(dt*dp13_dt(index+1)/2))
+ 1/2*1i*(Om23(index+1)+Om23(index+2))/2*
(p23(index+1)+(dt*dp23_dt(index+1)/2)-p32(index+1)-conj(dt*dp23_dt(index+1)/2));
    k2_12(index+1) = 1i*Delw21*(p12(index+1)+(dt*dp12_dt(index+1)/2))
- 1/2*1i*(Om23(index+1)+Om23(index+2))/2*(p13(index+1)+(dt*dp13_dt(index+1)/2))
+ 1/2*1i*(Om13(index+1)+Om13(index+2))/2*(p32(index+1)+(dt*dp23_dt(index+1)/2));
    k2_13(index+1) = 1i*Delw31*(p13(index+1)+(dt*dp13_dt(index+1)/2))
+ 1/2*1i*(Om13(index+1)+Om13(index+2))/2*
(p33(index+1)+(dt*dp33_dt(index+1)/2)-p11(index+1)-(dt*dp11_dt(index+1)/2))
- 1/2*1i*(Om23(index+1)+Om23(index+2))/2*(p12(index+1)+(dt*dp12_dt(index+1)/2));
    k2_23(index+1) = 1i*(Delw31-Delw21)*(p23(index+1)+(dt*dp23_dt(index+1)/2))
+ 1/2*1i*(Om23(index+1)+Om23(index+2))/2*
(p33(index+1)+(dt*dp33_dt(index+1)/2)-p22(index+1)-(dt*dp22_dt(index+1)/2))
-1/2*1i*(Om13(index+1)+Om13(index+2))/2*(p21(index+1)+conj(dt*dp12_dt(index+1)/2));

end

% Assembling into density matrix
% d_M =[p11: p21: p31;
%       p12: p22: p32;
%       p13: p23: p33]
d_M(:,1,1) = p11;
d_M(:,1,2) = p21;
d_M(:,1,3) = p31;
d_M(:,2,1) = p12;
d_M(:,2,2) = p22;
d_M(:,2,3) = p32;
d_M(:,3,1) = p13;
d_M(:,3,2) = p23;
d_M(:,3,3) = p33;
d_M(:,4,1) = c1.*ones(length(p11),1);
d_M(:,4,2) = c2.*ones(length(p11),1);
d_M(:,4,3) = c3.*ones(length(p11),1);
end
```